Effects of Cloud-Radiative Heating on AGCM Simulations of Convectively Coupled Equatorial Waves

Jia-Lin Lin[1], Myong-In Lee[2], Daehyun Kim[3], and In-Sik Kang[3]

[1]NOAA ESRL/CIRES Climate Diagnostics Center, Boulder, CO
[2]NASA GSFC Global Modeling and Assimilation Office, Greenbelt, MD
[3]School of Earth and Environmental Sciences, Seoul National University, Seoul, Korea

Corresponding author address: Dr. Jia-Lin Lin
NOAA ESRL/CIRES Climate Diagnostics Center
325 Broadway, R/PSD1, Boulder, CO 80305-3328
Email: jialin.lin@noaa.gov

Abstract

This study examines the effects of cloud-radiative heating on convectively coupled equatorial waves simulated by the Seoul National University (SNU) atmospheric general circulation model (AGCM). The strength of cloud-radiative heating is adjusted by modifying the autoconversion timescale, needed for cloud condensates to grow up to rain drops. Eight years of AMIP experiment for each model configuration are analyzed. Space-time spectral analysis is used to obtain the variance and phase speed of dominant convectively coupled equatorial waves, including the Madden-Julian Oscillation (MJO), Kelvin, equatorial Rossby (ER), mixed Rossby-gravity (MRG), and eastward inertio-gravity (EIG) and westward inertio-gravity (WIG) waves.

The results show that cloud-radiative heating has significant effect on the variance of the convectively coupled equatorial waves. The variance increases monotonically with decreasing cloud-radiative heating for Kelvin, MRG and WIG waves, but sometimes reaches a saturation value or even decreases for ER and EIG waves. Cloud-radiative heating has little effect on the prominence or phase speed of the waves.

1. Introduction

The tropical deep convection does not occur randomly, but is often organized by convectively coupled equatorial waves, such as the Madden-Julian Oscillation (Madden and Julian 1971), Kelvin, equatorial Rossby (ER), mixed Rossby-gravity (MRG), and eastward inertio-gravity (EIG) and westward inertio-gravity (WIG) waves (e.g. Takayabu 1994; Wheeler and Kiladis 1999, hereafter WK). These waves significantly affect a wide range of tropical weather such as the onset and breaks of the Indian and Australian summer monsoons (e.g. Yasunari 1979; Wheeler and McBride 2005), and the formation of tropical cyclones in almost all basins (e.g. Liebmann et al. 1994; Maloney and Hartmann 2001a; Bessafi and Wheeler 2006). On a longer timescale, the convectively coupled equatorial waves also trigger or terminate some El Nino events (e.g. Kessler et al. 1995, Takayabu et al. 1999, Bergman et al. 2001; Roundy and Kiladis 2006). Therefore, these waves are important for both weather prediction and climate prediction.

Unfortunately, these convectively coupled equatorial waves are not well simulated in the general circulation models (GCMs) used for predictions and projections. For example, poor simulation of the MJO has been a well-known long-standing problem in GCMs, and the model MJOs are often too weak and propagate too fast (e.g. Hayashi and Sumi 1986; Hayashi and Golder 1986, 1988, Lau et al. 1988, Slingo et al. 1996; Waliser et al. 2003; Lin et al. 2006). The Atmospheric Model Intercomparison Project (AMIP) study by Slingo et al. (1996) found that no model has captured the dominance of the MJO in space-time spectral analysis found in observations, and nearly all have relatively more power at higher frequencies (<30 days) than in observations. Recently, Lin et al. (2006) evaluates the tropical intraseasonal variability in 14 coupled GCMs participating in the

Inter-governmental Panel on Climate Change (IPCC) Fourth Assessment Report (AR4). The results show that current state-of-the-art GCMs still have significant problems and display a wide range of skill in simulating the tropical intraseasonal variability. Most of the models produce overly weak MJO variance and poor MJO propagation. Moreover, the MJO variance in 13 of the 14 models does not come from a pronounced spectral peak, but usually comes from part of an over-reddened spectrum, which in turn is associated with too-strong persistence of equatorial precipitation.

Lin et al. (2006) also evaluated, for the first time in literature, other convectively coupled equatorial waves simulated by the GCMs. About half of the models have signals of convectively coupled equatorial waves, with Kelvin and MRG-EIG waves especially prominent. However, the variances are generally too weak for all wave modes except the EIG wave, and the phase speeds are generally too fast, suggesting that these models may not have a large enough reduction in their "effective static stability" by diabatic heating.

It is widely accepted that wave-heating feedback is central for the amplification and maintenance of the convectively coupled equatorial waves. The total diabatic heating has two main components: convective heating (release of latent heat, along with eddy flux divergences that shape the profile) and radiative heating. Most theoretical studies have focused only on the role of convective heating in wave-heating feedback. The mechanisms studied include the wave-CISK (conditional instability of the second kind) mechanism (e.g., Lau and Peng 1987), the wind-induced surface heat exchange (WISHE) mechanism (e.g., Emanuel 1987; Neelin et al. 1987), and the charge–discharge mechanism (e.g., Blade and Hartmann 1993; Hayashi and Golder 1997).

The radiative heating, on the other hand, also contribute significantly to the total diabatic heating and thus may affect the convectively coupled equatorial waves. The radiative heating has two aspects: column-integrated heating and vertical heating profile, which have different effects on deep convection. The column-integrated heating tends to enhance the convective heating because in the convectively active phase of an convectively coupled equatorial wave, clouds and water vapor associated with deep convection reduce outgoing longwave radiation (OLR) to space and therefore increase radiative heating in the atmosphere. As a quantitative measure, an enhancement factor of radiative heating can be defined as the ratio between the column-integrated radiative heating and the column-integrated convective heating. Using collocated top-of-atmosphere (TOA) and surface radiative flux measurements from special field program data and long-term TOA flux data, Lin and Mapes (2004) examined the column-integrated radiation budget of the MJO, and found that the column-integrated radiative heating is nearly in phase with the precipitation and enhances the net condensation heating by about 10%–15%, with the dominant contribution from the reduction of OLR during wet periods. Recently, several modeling studies found that radiative heating can also significantly affect the amplitude and/or phase speed of the simulated intraseasonal oscillations (e.g. Raymond 2001; Sobel and Gildor 2003; Bony and Emanuel 2005). In an idealized model of thermodynamic atmosphere–ocean interaction on the intraseasonal time scale, Sobel and Gildor (2003) found that the enhancement factor of radiative heating is the most sensitive parameter, and both the growth rate and the period of simulated intraseasonal oscillations increase with the enhancement factor. In a theoretical model, Raymond (2001) demonstrated that when the enhancement factor is very large the

radiative heating can reduce the effective static stability to a negative value, that is, to an effective static instability. He termed this instability the radiative–convective instability. An MJO-like slow eastward-propagating mode appears to develop in his model from this radiative–convective instability.

The second aspect of radiative heating is its vertical heating profile. Using the TOGA COARE radiative heating profiles calculated by Qian (2003), Lin et al. (2004) analyzed the vertical structure of radiative heating in the MJO. They found that during the convectively active phase, radiative heating is characterized by warming in the lower and middle troposphere but cooling in the upper troposphere. Such a heating profile tends to suppress deep convection, in contrast to the enhancing effect of column-integrated heating. Several previous GCM studies found that cloud radiative heating tends to suppress the simulated MJO-like mode (e.g. Slingo and Madden 1991; Lee et al. 2001). Lee et al. (2001) conducted two types of simulation: one with prescribed zonal mean radiation and the other with fully interactive clouds and radiation. In contrast to the fixed radiation case, where the MJO is simulated reasonably well, the cloud-radiation interaction significantly contaminates the eastward propagation of the MJO by producing small-scale disturbances moving westward with the easterly basic winds. The small-scale disturbances are persistently excited by a strong positive feedback through interaction between cumulus-anvil clouds and radiation. The longwave interaction is shown to play a bigger role in contaminating the MJO than the shortwave interaction does. The anvil clouds reduce the longwave cooling significantly in the lower troposphere while releasing latent heating in the upper troposphere. To moderate the strong cloud-radiation feedback, the large-scale condensation scheme in the GCM is modified by reducing the

autoconversion timescale, needed for cloud condensates to grow up to rain drops. In addition, upper air ice cloud contents are reduced to change the cloud albedo. These modifications make a more realistic simulation of the MJO similar to the observed. However, the effects of cloud radiative heating on AGCM-simulated other convectively coupled equatorial waves (e.g. Kelvin, ER, and MRG waves) have not been studied.

The purpose of this study is to extend the Lee et al. (2001) study to examine the effects of cloud radiative heating on AGCM-simulated convectively coupled equatorial waves. Following Lee et al. (2001), the strength of cloud radiative heating is adjusted by modifying the autoconversion timescale, needed for cloud condensates to grow up to rain drops. The questions we address are: *Are the AGCM-simulated convectively coupled equatorial waves sensitive to the strength of cloud radiative heating? Does cloud radiative heating enhance or suppress the waves?*

The models and validation datasets used in this study are described in section 2. The diagnostic methods are described in section 3. Results are presented in section 4. A summary and discussion are given in section 5.

2. Models and validation datasets

The model used in this study is the Seoul National University atmospheric general circulation model (SNUGCM). The model is a global spectral model, with 20 vertical levels in a sigma coordinate. In this study, T42 ($\sim$2.8^o x 2.8^o) truncation is used for the model horizontal resolution. Moist convection is represented by the simplified version of the Relaxed Arakawa-Schubert (RAS) formulation (Numaguti et al. 1995). The large-scale condensation scheme consists of a prognostic microphysics parameterization for

total cloud liquid water (Le Treut and Li, 1991) with a diagnostic cloud fraction parameterization. Non-precipitating shallow convection scheme (Tiedtke 1983) is also implemented in the model for the mid-tropospheric moist convection. The boundary layer scheme is a non-local diffusion scheme based on Holtslag and Boville (1993), while the land surface model is from Bonan (1996). The radiation process is parameterized by the two-stream k distribution scheme implemented by Nakajima et al. (1995). Other details of the model physics are described in Lee et al. (2001, 2003).

To examine the effects of cloud radiative heating on the simulated convectively coupled equatorial waves, we tested the parameter sensitivity to the autoconversion timescale in the large-scale condensation scheme. As discussed in Lee et al. (2001), this parameter gives a characteristic time for auto-conversion of cloud droplets into precipitating rain drops. As it becomes smaller, the precipitating process is faster with shorter cloud lifetime. This can effectively reduce the magnitude of the cloud-radiative heating (Lee et al. 2001). In this study, several different values were tested for the timescale originally set to 9600 seconds, which are listed in Table 1. In each experiment, the minimum entrainment constraint in the RAS convection scheme was commonly applied with a positive constant $\alpha=0.1$, which is same as in Lee et al. (2001). Each run consists of 8 year AMIP-style simulations (1979-1986) driven by the same observed sea surface temperatures and sea-ice distributions.

The effect of changing the autoconversion timescale on the cloud-radiative heating is shown in Figure 1, which plots the linear regression of daily –OLR versus precipitation along the equator (5N-5S) for observation and the different model experiments. As shown by Lin and Mapes (2004), OLR perturbation is the dominant component of the

column-integrated cloud-radiative heating, while precipitation corresponds to the column-integrated latent heating, and thus their ratio is a good approximation of the enhancement factor discussed in the introduction. In observation (AVHRR OLR versus GPCP 1DD precipitation), the enhancement factor is about 14%, which is consistent with the results of Lin and Mapes (2004) using different observational datasets. In the model, when the autoconversion timescale decreases, the enhancement factor significantly decreases.

The model simulations are validated using multiple observational datasets. To bracket the uncertainties associated with precipitation measurements/retrievals, especially the well-known difference between infrared (IR) based retrievals and microwave-based retrievals (e.g. Yuter and Houze 2000), we use two different precipitation datasets: (1) 8 years (1997-2004) of daily GOES Precipitation Index (GPI, Janowiak and Arkin 1991) precipitation with a horizontal resolution of 2.5 degree longitude by 2.5 latitude, which is retrieved based on IR measurements from multiple geostationary satellites; and (2) 8 years (1997-2004) of daily Global Precipitation Climatology Project (GPCP) One-Degree-Daily (1DD) Precipitation (Huffman et al. 2001) with a horizontal resolution of 1 degree longitude by 1 degree latitude. These are IR-based GPI retrievals scaled by the monthly means of microwave-based SSM/I retrievals.

3. **Method**

Through the space-time spectral analysis of outgoing longwave radiation (OLR), Takayabu (1994) and WK demonstrated that a significant portion of tropical cloudiness is organized in waves corresponding to the normal modes of the linear shallow water

system isolated by Matsuno (1966). In WK, these spectra represent the power remaining in the symmetric and antisymmetric components of OLR about the equator after dividing raw wavenumber-frequency power spectra by an estimate of the background power spectrum. Peaks standing above the background correspond to the Kelvin, n=1 equatorial Rossby (ER), mixed Rossby-gravity (MRG), n=0 eastward inertio-gravity (EIG), n=1 westward inertio-gravity (WIG) and n=2 WIG waves. It was found that the dispersion curves that best match the wavenumber-frequency characteristics of these waves have surprisingly shallow equivalent depths in the range of around 25 m, which is about an order of magnitude smaller than that expected for a free wave with a similar vertical wavelength twice the depth of the troposphere (e.g. Salby and Garcia 1987; Wheeler et al. 2000).

Using the methodology of WK, space-time spectra of daily tropical precipitation were obtained for the 8 years of model data used in this study and compared with those of eight years of observed precipitation estimates from the GPI and 1DD data sets. We will briefly outline this procedure here, and refer the reader to WK and Lin et al. (2006) for further details.

The model and validation precipitation data were first interpolated to a zonal resolution of 5 degrees longitude with the latitudinal resolution. We first decomposed the precipitation into its antisymmetric and symmetric components, averaged these from 15N to 15S, and computed spectra of the averaged values. To reduce noise the space-time spectra were calculated as in WK for successive overlapping segments of data and then averaged, here 128 days long with 78 days of overlap between each segment. Complex Fourier coefficients are first obtained in zonal planetary wavenumber space, which are

then subjected to a further complex FFT to obtain the wavenumber-frequency spectrum for the symmetric and antisymmetric components of precipitation about the equator.

An estimate of the "background" space-time spectrum is obtained for each data set by averaging the power of the symmetric and antisymmetric spectra and smoothing this by successive passes of a 1-2-1 filter in frequency and wavenumber (see WK). The raw spectra are then divided by this background to obtain an estimate of the signal standing above the background noise. Here we assume the signal is significant if it stands at 1.2 times (or 20% above) the background. It should be emphasized that, while this is only a rough estimate of the true "significance" of the signals, the intent is to simply identify those modes which might represent signals in rainfall standing above a simple red noise continuum that would presumably prevail if rainfall were not organized by disturbances on the large scale.

The definitions of Kelvin, ER, MRG, EIG and WIG modes are as in WK and Lin et al. (2006). Each mode was isolated by filtering in the wavenumber-frequency domain (see Fig. 6 of WK for the defined regions of filtering for each wave), and the corresponding time series were obtained by an inverse space-time Fourier transform.

As in Lin et al. (2006) the MJO is defined as significant rainfall variability in eastward wavenumber 1-6 and in the period range of 30-70 days. The variance of the MJO anomaly was also compared with the variance of its westward counterpart, i.e., the westward wavenumbers 1 through 6, 30-70 day anomaly, which was isolated using the same method as above.

4. Results

a Climatological precipitation in the equatorial belt

Previous observational studies indicate that the intraseasonal variance of convection is highly correlated with time-mean convective intensity (e.g. WK, Hendon et al. 1999). Therefore we first look at the eight-year time-mean precipitation along the equatorial belt, especially over the Indo-Pacific warm pool region, where most of the convectively coupled equatorial waves have the largest variance (WK). Figure 2 shows the annual mean precipitation versus longitude averaged between (a) 15N and 15S, and (b) 5N and 5S. To focus on the large-scale features, we smoothed the data zonally to retain only zonal wavenumbers 0 through 6. Figure 2 demonstrates two points. First, all experiments simulate reasonably the basic feature of observed precipitation, with the primary maximum over the Indo-Pacific warm pool region, and a secondary local maximum over Central/South America. Within the warm pool region, all experiments also reproduce the local minimum of precipitation over the maritime continent, but there is a positive bias over the western Pacific and a negative bias over the eastern Indian Ocean. Outside the warm pool region, all experiments produce quite realistic magnitude of precipitation over Central/South America. Comparing with the 15N-15S average (Figure 2a), the biases in 5N-5S average (Figure 2b) are smaller over western Pacific, but larger over eastern Indian Ocean. Second, changing the precipitation timescale does not change much the mean precipitation, and thus any difference in the intraseasonal variability is likely due to change in cloud-radiation feedback instead of change in mean precipitation.

In short, the climatological precipitation over the Indo-Pacific warm pool is reasonably simulated by all experiments. Changing the precipitation timescale has little

12

effect on the climatological mean precipitation, suggesting that any related change in intraseasonal variability is likely due to change in cloud-radition feedback instead of change in mean precipitation.

b   Total intraseasonal (2-128 day) variance

Figure 3 shows the total variance of the 2-128 day precipitation anomaly along the equator averaged between (a) 15N-15S, and (b) 5N-5S. There are two important things to note concerning Figure 3. First, the total intraseasonal variance in all experiments is overly large over western Pacific, although it is overly small over Indian Ocean. This is very encouraging because 13 of the 14 IPCC AR4 GCMs analyzed by Lin et al. (2006) produce overly small variance over both western Pacific and Indian Ocean, although their annual mean precipitation is often as large as in the SNU model studied here. Second, reducing the precipitation timescale (i.e. reducing cloud-radiative heating) has little effect on the total intraseasonal variance over western Pacific or Indian Ocean, although it does enhance significantly the variance over the continents such as Africa and South America.

c   Dominant intraseasonal modes

Figure 4 and Figure 5 show the results of dividing the symmetric and antisymmetric raw spectra by the estimates of their background spectra. This normalization procedure removes a large portion of the systematic biases within the various models and observed data sets, more clearly displaying the model disturbances with respect to their own climatological variance at each scale. Signals of the Kelvin, ER, and WIG waves are readily identified in the observational symmetric spectra (Figure 4a and b), along with the MRG and EIG waves in the antisymmetric spectra (Figure 5a and b). The MJO also appears as a prominent signal, especially in the symmetric spectra. Dispersion curves of

the shallow water modes are also shown on all spectra, corresponding to equivalent depths of 12, 25, and 50 m. As in the OLR spectra of WK, all of the observed spectral peaks corresponding to shallow water modes best match an equivalent depth of around 25 m in the observational rainfall data.

All experiments produce prominent signals of convectively coupled equatorial waves, with Kelvin and MRG-EIG waves especially prominent. The phase speed is quite realistic for all the wave modes except the EIG wave which displays a too-fast phase speed. Changing the precipitation timescale has little effect on the prominence or phase speed of the convectively coupled equatorial waves. Nevertheless, the fairly good simulation of convectively coupled equatorial waves by the SNUGCM support our use of it to examine the effect of cloud-radiation feedback on the waves.

When a model displays signals of a certain wave mode in Figure 4 and Figure 5, it means that the variance of that wave mode stands out above the background spectra (i.e., a high signal-to-noise ratio), but the absolute value of the variance of that wave mode may not be large. Therefore, it is of interest to look further at the absolute values of the variance of each wave mode. Figure 6 shows the variances of the (a) Kelvin, (b) ER, (c) MRG, (d) EIG, and (e) WIG modes along the equator averaged between 15N and 15S. Changing the precipitation timescale significantly affects the variance of the various wave modes. For Kelvin (Figure 6a), MRG (Figure 6c) and WIG (Figure 6e) waves, the variance increases monotonically with decreasing precipitation timescale (i.e. decreasing cloud-radiative heating). However, for the ER wave (Figure 6b), the variance increases from CNTL to EXP1, but seems to reach a saturation value at EXP1 and does not change when precipitation timescale further decreases. For EIG wave (Figure 6d), the variance

14

increases from CNTL to EXP1, remain nearly the same from EXP1 to EXP2, then decreases significantly from EXP2 to EXP3.

In summary, all experiments produce prominent signals of convectively coupled equatorial waves, with Kelvin and MRG-EIG waves especially prominent and the phase speeds generally quite realistic. These support our use of the SNUGCM to examine the effect of cloud-radiation feedback on the convectively coupled equatorial waves. Changing the precipitation timescale (cloud-radiative heating) has little effect on the prominence or phase speed of the waves, but has significant effects on the variance of the waves. The variance increases monotonically with decreasing cloud-radiative heating for Kelvin, MRG and WIG waves, but sometimes reaches a saturation value or even decreases with decreasing cloud-radiative heating for ER and EIG waves.

5. Summary and discussion

This study examines the effects of cloud-radiative heating on convectively coupled equatorial waves simulated by the SNU AGCM. The strength of cloud-radiative heating is adjusted by modifying the autoconversion timescale, needed for cloud condensates to grow up to rain drops. Eight years of AMIP experiment for each model configuration are analyzed. Space-time spectral analysis is used to obtain the variance and phase speed of dominant convectively coupled equatorial waves, including the MJO, Kelvin, ER, MRG, EIG and WIG waves.

The results show that cloud-radiative heating has significant effect on the variance of the convectively coupled equatorial waves. The variance increases monotonically with decreasing cloud-radiative heating for Kelvin, MRG and WIG waves, but sometimes

reaches a saturation value or even decreases for ER and EIG waves. Cloud-radiative heating has little effect on the prominence or phase speed of the waves.

The main finding of this study is that cloud-radiative heating tends to suppress AGCM-simulated convectively coupled equatorial waves. As discussed in the introduction, the cloud-radiative heating has two aspects which have opposite effect on convective heating: the column-integrated cloud-radiative heating enhances the convective heating, but the vertical profile of cloud-radiative heating tends to suppress deep convection and convective heating. Therefore, modeling studies are needed to determine the sign of the net effect. Most of the theoretical modeling studies mainly considered the first effect, i.e., the enhancing effect of column-integrated heating (e.g. Raymond 2001; Sobel and Gildor 2003; Bony and Emanuel 2005). The GCM experiments, on the other hand, consider both the enhancing effect of column-integrated heating and the suppressing effects of vertical radiative heating profile. The radiative heating profiles in our model experiments have been analyzed by Lee et al. (2001) and are quite similar to those derived from observational data (e.g. Qian 2003). Our results show that the net effect of radiative heating is suppressing most of the convectively coupled equatorial waves, suggesting that the effect of vertical heating profile dominates over that of the column-integrated heating.

Our results have important implications for improving GCM simulations of convectively coupled equatorial waves and MJO. The cloud-radiative fluxes and heating in GCMs are often tuned to match the observed TOA and surface fluxes, and our results suggest that such tuning may have strong effects on the simulated convectively coupled

equatorial waves and MJO. Therefore, caution should be taken when such tuning is conducted.

REFERENCES

Bergman, J. W., H. H. Hendon, K. M.Weickmann, 2001: Intraseasonal Air-Sea Interactions at the Onset of El Nino. *J. Climate*, **14**, 1702-1719.

Bessafi, M. and M.C. Wheeler, 2005: Modulation of south Indian Ocean tropical cyclones by the Madden-Julian oscillation and convectively-coupled equatorial waves. *Mon. Wea. Rev.*, in press.

Bonan, G. B., A land surface model (LSM version 1.0) for ecological, hydrological, and atmospheric studies: Technical description and user's guide. NCAR *Tech. Note NCAR/TN-417+STR,* Natl. Cent. For Atmos. Res., 150pp., Boulder, Colorado.

Bony, S., and Kerry A. Emanuel, 2005: On the Role of Moist Processes in Tropical Intraseasonal Variability: Cloud–Radiation and Moisture–Convection Feedbacks. J. Atmos. Sci., 62, 2770-2789.

Dickinson, M., and Molinari J., 2002: Mixed Rossby–gravity waves and western Pacific tropical cyclogenesis. Part I: Synoptic evolution. *J. Atmos. Sci.,* **59**, 2183–2196.

Duchan, C.E., 1979: Lanczos filtering in one and two dimensions. *J. Appl. Meteor.*, **18**, 1016-1022.

Emanuel, K. A., J. D. Neelin, and C. S. Bretherton, 1994: On large-scale circulations in convecting atmospheres. *Quart. J. Roy. Meteor. Soc.,* **120,** 1111–1143.

Haertel, P. T., and G. N. Kiladis, 2004: On the dynamics of two-day equatorial disturbances. *J. Atmos. Sci.*, submitted.

Hayashi, Y., and A. Sumi, 1986: The 30-40 day oscillation simulated in an"aqua planet" model. *J. Meteor. Soc. Japan.*, **64**, 451-466.

Hayashi, Y., and D. G. Golder, 1986: Tropical intraseasonal oscillations appearing in a
GFDL general circulation model and FGGE data. Part I: Phase propagation. *J. Atmos.
Sci.*, **43**, 3058-3067.

Hayashi, Y., and D. G. Golder, 1988: Tropical intraseasonal oscillations appearing in a
GFDL general circulation model and FGGE data. Part II: Structure. *J. Atmos. Sci.*, **45**,
3017-3033.

Hendon, H.H., C. Zhang, and J.D. Glick, 1999: Interannual variation of the MJO during
austral summer. *J. Climate*, **12**, 2538-2550.

Holtslag, A. A. M., and B. A. Boville, 1993: Local versus nonlocal boundary layer
diffusion in a global climate model. *J. Clim.*, **6**, 1825-1642.

Huffman, G.J., R.F. Adler, M.M. Morrissey, S. Curtis, R. Joyce, B. McGavock, and J.
Susskind, 2001: Global precipitation at one-degree daily resolution from multi-
satellite observations. *J. Hydrometeor.*, **2**, 36-50.

Janowiak, J. E., and P. A. Arkin, 1991: Rainfall variations in the Tropics during 1986-
1989, as estimated from observations of cloud-top temperatures. *J. Geophys. Res.*, **96**
(Suppl.), 3359-3373.

Kessler, W. S., and M. J. McPhaden, and K. M. Weickmann, 1995: Forcing of
intraseasonal Kelvin waves in the equatorial Pacific. *J. Geophys. Res.*, **100**, 10613-
10631.

Knutson, T. R., and K. M. Weickmann, 1987: 30–60 Day Atmospheric Oscillations:
Composite Life Cycles of Convection and Circulation Anomalies. *Monthly Weather
Review*, 115, 1407–1436.

Knutson, T. R., Klaus M. Weickmann and John E. Kutzbach. 1986: Global-Scale Intraseasonal Oscillations of Outgoing Longwave Radiation and 250 mb Zonal Wind during Northern Hemisphere Summer. *Monthly Weather Review*, 114, 605–623.

Lau, K. M., and P. H. Chan, 1985: Aspects of the 40-50-day oscillation during the northern winter as inferred from outgoing longwave radiation. *Mon. Wea. Rev.*, **113**, 1889-1909.

Lau, N. C., I. M. Held, and J. D. Neelin, 1988: The Madden-Julian oscillations in an idealized general circulation model. *J. Atmos. Sci.*, **45**, 3810-3831.

Lee, M.-I., I.-S. Kang, J.-K. Kim, and B. E. Mapes, 2001: Influence of cloud-radiation interaction on simulating tropical intraseasonal oscillation with an atmospheric general circulation model , *J. Geophys. Res.*, **106**, 14219-14233.

Lee, M.-I., I.-S. Kang, and B.E. Mapes, 2003: Impacts of cumulus convection parameterization on aqua-planet AGCM simulations of tropical intraseasonal variability. *J. Meteor. Soc. Japan,* **81**, 963-992.

Le Treut, H., and Z. −X. Li, 1991: Sensitivity of an atmospheric general circulation model to prescribed SST changes: feedback effects associated with the simulation of cloud optical properties. *Clim. Dyn.*, 5, 175-187.

Liebmann, B., H. H. Hendon, and J. D. Glick, 1994: The relationship between tropical cyclones of the western Paci.c and Indian Oceans and the Madden-Julian oscillation. *J. Meteor. Soc. Japan*, **72**, 401-411.

Liebmann, B., and C. A. Smith, 1996: Description of a complete (interpolated) outgoing longwave radiation dataset. *Bull. Amer. Meteor. Soc.*, **77**, 1275-1277.

Lin, J. L., 2006: The double-ITCZ problem in IPCC AR4 coupled GCMs: Ocean-atmosphere feedback analysis. *J. Climate*, accepted with minor revisions. Pdf file available at http://www.cdc.noaa.gov/people/jialin.lin/

Lin, J. L., and B. E. Mapes, 2004: Radiation budget of the tropical intraseasonal oscillation. *J. Atmos. Sci.*, **61**, 2050-2062.

Lin, J. L., B. E. Mapes, M. H. Zhang and M. Newman, 2004: Stratiform precipitation, vertical heating profiles, and the Madden-Julian Oscillation. *J. Atmos. Sci.*, **61**, 296-309.

Lin, J. L., M. H. Zhang, and B. E. Mapes, 2005: Zonal momentum budget of the Madden-Julian Oscillation: The sources and strength of equivalent linear damping. *J. Atmos. Sci.*, **62**, 2172-2188.

Lin, J. L., G.N. Kiladis, B.E. Mapes, K.M. Weickmann, K.R. Sperber, W.Y. Lin, M. Wheeler, S.D. Schubert, A. Del Genio, L.J. Donner, S. Emori, J.-F. Gueremy, F. Hourdin, P.J. Rasch, E. Roeckner, and J.F. Scinocca, 2006: Tropical intraseasonal variability in 14 IPCC AR4 climate models. Part I: Convective signals. *J. Climate*, **19**, 2665-2690.

Madden, R. A., and P. R. Julian, 1971: Detection of a 40-50 day oscillation in the zonal wind in the tropical Paci.c. *J. Atmos. Sci.*, **28**, 702-708.

Madden, R. A., and P. R. Julian, 1972: Description of global-scale circulation cells in the tropics with a 40-50 day period. *J. Atmos. Sci.*, **29**, 1109-1123.

Madden, R. A., and P. R. Julian, 1994: Observations of the 40-50-day tropical oscillation-A review. *Mon. Wea. Rev.*, **122**, 814-837.

Maloney, E. D., and D. L. Hartmann, 2000: Modulation of eastern North Pacific hurricanes by the Madden–Julian oscillation. *J. Climate.,* **13**, 1451–1460.

Maloney, E. D., Hartmann, D. L. 2001: The Madden-Julian Oscillation, Barotropic Dynamics, and North Pacific Tropical Cyclone Formation. Part I: Observations. *J. Atmos. Sci.*, **58**, 2545-2558.

Mapes, B. E., and R. A. Houze, 1995: Diabatic divergence profiles in western Pacific mesoscale convective systems. *J. Atmos. Sci.*, **52**, 1807-1828.

Mapes, B. E., and J. L. Lin, 2005: Doppler radar observations of mesoscale wind divergence in regions of tropical convection. *Mon. Wea. Rev.*, in press.

Moorthi, S., and Suarez M. J., 1992: Relaxed Arakawa–Schubert: A parameterization of moist convection for general circulation models. *Mon. Wea. Rev.,* **120**, 978–1002.

Murakami, M., 1979: Large-scale aspects of deep convective activity over the GATE area. *Mon. Wea. Rev.*, **107**, 994-1013.

Nakajima, T., M. Tsukamoto, Y. Tsushima, and A. Numaguti, 1995: Modelling of the radiative processes in an AGCM, in *Climate System Dynamics and Modelling*, vol. I-3, edited by T. Matsuno, pp. 104-123, Univ. of Tokyo, Tokyo.

Neelin, J. D., and I. M. Held. 1987: Modeling Tropical Convergence Based on the Moist Static Energy Budget. *Monthly Weather Review*, 115, 3–12.

Numaguti, A., M. Takahashi, T. Nakajima, and A. Sumi, 1995: Development of an atmospheric general circulation model, in *Climate System Dynamics and Modelling*, vol. I-3, edited by T. Matsuno, pp. 1-27, Univ. of Tokyo, Tokyo.

Oort, A. H., and J. J. Yienger, 1996: Observed long-term variability in the Hadley circulation and its connection to ENSO. *J. Climate*, **9**, 2751-2767.

Qian T., 2003: Cloud vertical structure and radiative heating profiles during TOGA COARE. Ph.D. thesis, State University of New York at Stony Brook, 141 pp. [Available from State University of New York at Stony Brook, Stony Brook, NY 11794.].

Raymond D. J., 2001: A new model of the Madden–Julian oscillation. *J. Atmos. Sci*, **58**, 2807–2819.

Salby, M., and R. R. Garcia, 1987: Transient response to localized episodic heating in the tropics. Part I : Excitation and short-time near-field behavior. *J. Atmos. Sci*., **44**, 458-498

Schubert, S., R. Dole, H.v.d. Dool, M. Suarez, and D. Waliser, 2002: Proceedings from a workshop on "Prospects for improved forecasts of weather and short-term climate variability on subseasonal (2 week to 2 month) time scales", 16-18 April 2002, Mitchellville, MD, NASA/TM 2002-104606, vol. 23, pp. 171.

Slingo, J. M., and R. A. Madden, 1991: Characteristics of the tropical intraseasonal oscillation in the NCAR community climate model. *Q. J. R. Meteorol. Soc*., **117**, 1129-1169.

Slingo, J. M., and Coauthors, 1996: Intraseasonal oscillations in 15 atmospheric general circulation models: Results from an AMIP diagnostic subproject. *Climate Dyn.*, **12**, 325-357.

Sobel A. H., and H. Gildor, 2003: A simple time-dependent model of SST hot spots. *J. Climate*, **16**, 3978–3992.

Takayabu, Y. N., 1994: Large-scale cloud disturbances associated with equatorial waves. Part I: Spectral features of the cloud disturbances. *J. Meteor. Soc. Japan,* **72,** 433–448.

Takayabu, Y .N., T. Iguchi, M. Kachi, A. Shibata, and H. Kanzawa, 1999: Abrupt termination of the 1997-98 El Nino in response to a Madden-Julian oscillation. *Nature*, **402**, 279-282.

Tiedtke, M., 1983: The sensitivity of the time-mean large-scale flow to cumulus convection in the ECMWF model. *Workshop on Convection in Large-Scale Numerical Models*. ECMWF, 28 Nov-1 Dec 1983, pp297-316.

Tiedke, M., 1989: A comprehensive mass flux scheme for cumulus parameterization in large-scale models. *Mon. Wea. Rev.,* **117**, 1779-1800.

Tokioka, T., K. Yamazaki, A. Kitoh, and T. Ose, 1988: The equatorial 30-60-day oscillation and the Arakawa-Schubert penetrative cumulus parameterization. *J. Meteor. Soc. Japan*, **66**, 883-901.

Waliser, D., S. Schubert, A. Kumar, K. Weickmann, and R. Dole, 2003: Proceedings from a workshop on "Modeling, Simulation and Forecasting of Subseasonal Variability", NASA/CP 2003-104606, vol. 25, pp. 62.

Wang, B., and H. L. Rui, 1990: Synoptic climatology of transient tropical intraseasonal convective anomalies: 1975-1985. *Meteor. Atmos. Phys*., **44**, 43-61.

Wang, W., and M.E. Schlesinger, 1999: The dependence on convective parameterization of the tropical intraseasonal oscillation simulated by the UIUC 11-layer atmospheric GCM. *J. Climate*, **12**, 1423-1457.

Weickmann, K. M., G. R. Lussky, and J. E. Kutzbach, 1985: Intraseasonal (30-60 day) fluctuations of outgoing longwave radiation and 250 mb streamfunction during northern winter. *Mon. Wea. Rev.*, **113**, 941-961.

Weickmann, K., G. Kiladis and P. Sardeshmukh, 1997: The dynamics of intraseasonal atmospheric angular momentum oscillations. J. Atmos. Sci., 54, 1445-1461.

Wheeler, M., and G.N. Kiladis, 1999: Convectively Coupled Equatorial Waves: Analysis of Clouds and Temperature in the Wavenumber-Frequency Domain. *J. Atmos. Sci.,* **56**, 374-399.

Wheeler, M., G.N. Kiladis, and P.J. Webster, 2000: Large-scale dynamical fields associated with convectively coupled equatorial waves. *J. Atmos. Sci.*, 57, 613-640.

Wheeler, M.C., and J.L. McBride, 2005: Australian-Indonesian monsoon. *Intraseasonal Variability in the Atmosphere-Ocean Climate System.* W.K.M. Lau and D.E. Waliser (Eds.), Praxis Publishing, pp 125-173.

Yasunari, T., 1979: Cloudiness fluctuations associated with the northern hemisphere summer monsoon. *J. Meteor. Soc. Japan*, **57**, 227-242.

Yuter, S. E., and R. A. Houze Jr.. 2000: The 1997 Pan American Climate Studies Tropical Eastern Pacific Process Study. Part I: ITCZ Region. *Bulletin of the American Meteorological Society*, 81, 451–481.
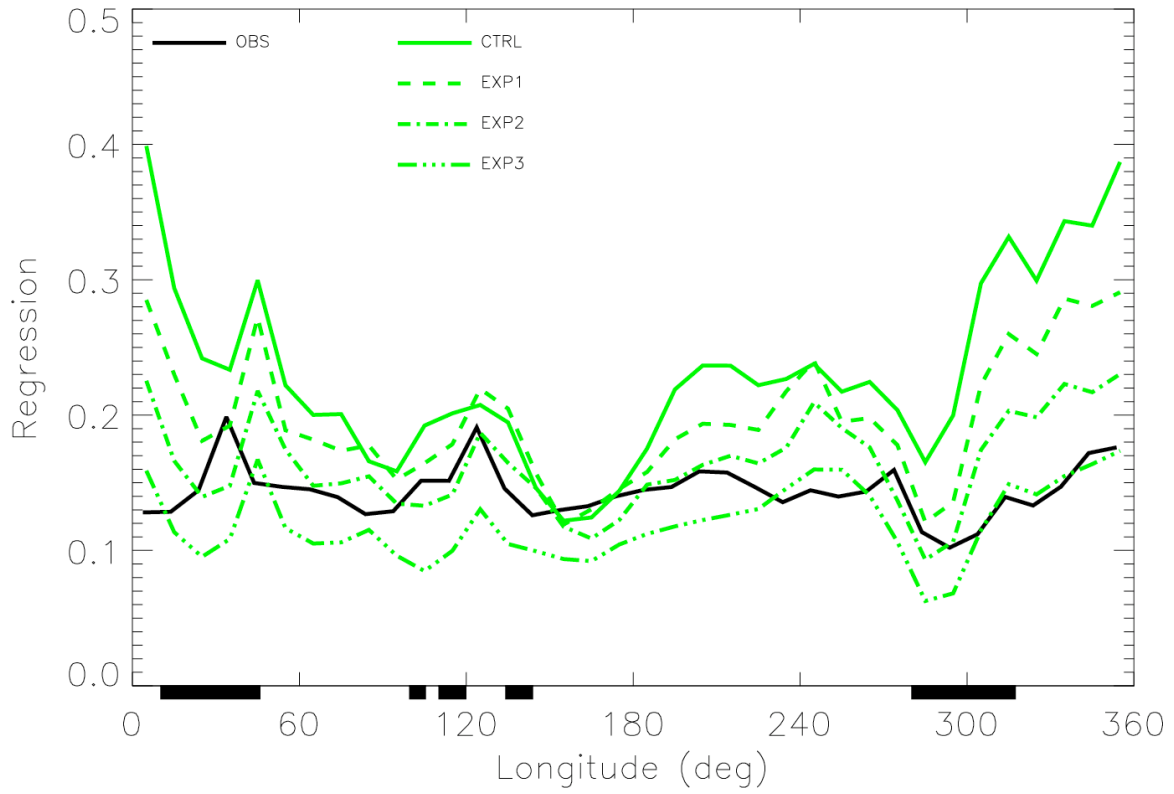
FIGURE CAPTIONS

Figure 1. Linear regression of daily -OLR vs precipitation along the equator averaged between 5N-5S for observation and model experiments. Same unit is used for both variables so that the regression coefficient is unitless.
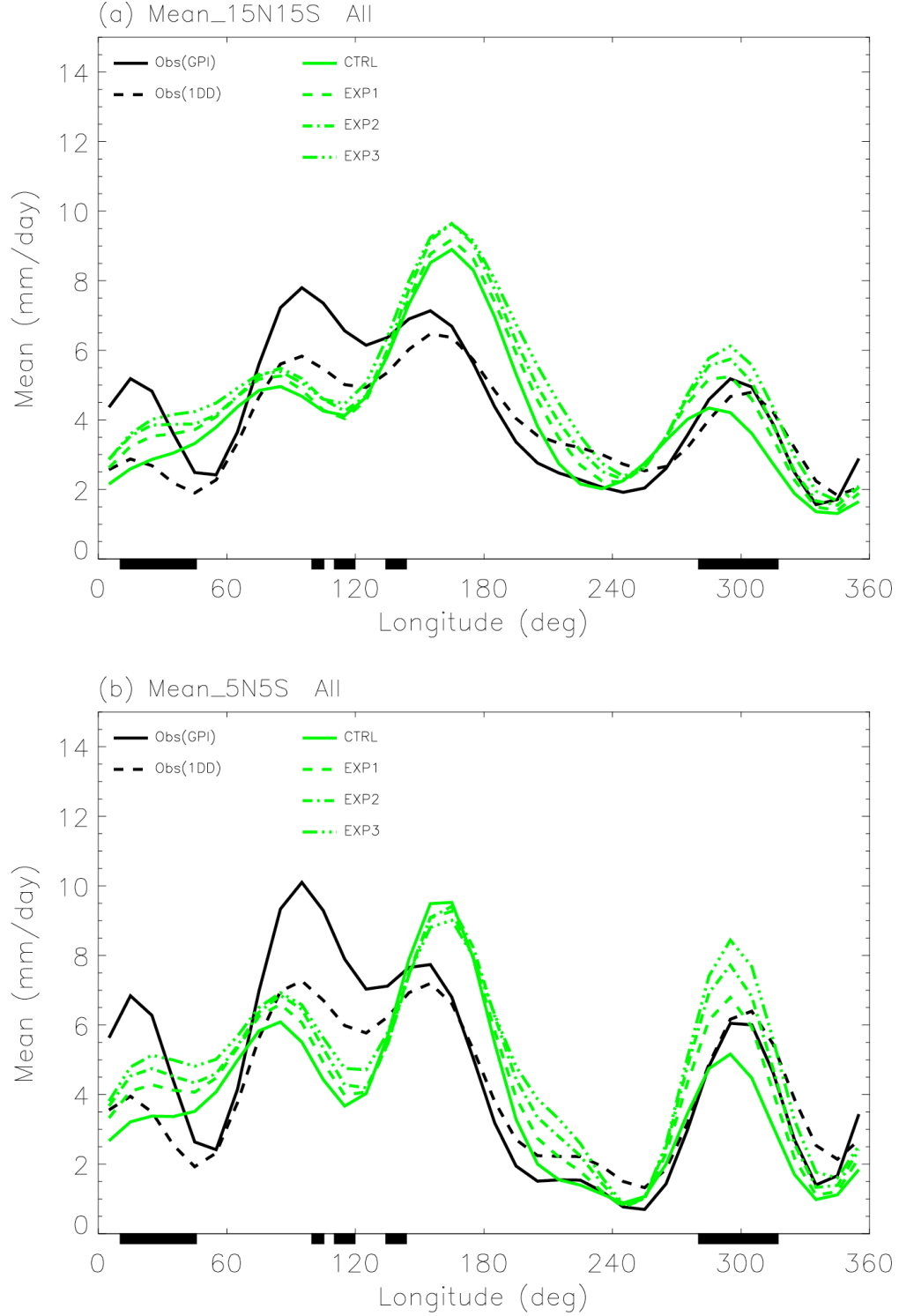
Figure 2. Annual mean precipitation along the equatorial belt averaged between (a) 15N and 15S, and (b) 5N and 5S for two observational datasets and each model experiment. The data are smoothed zonally to keep only wavenumber 0-6. The locations of continents within the equatorial belt are indicated by black bars under the abscissa.
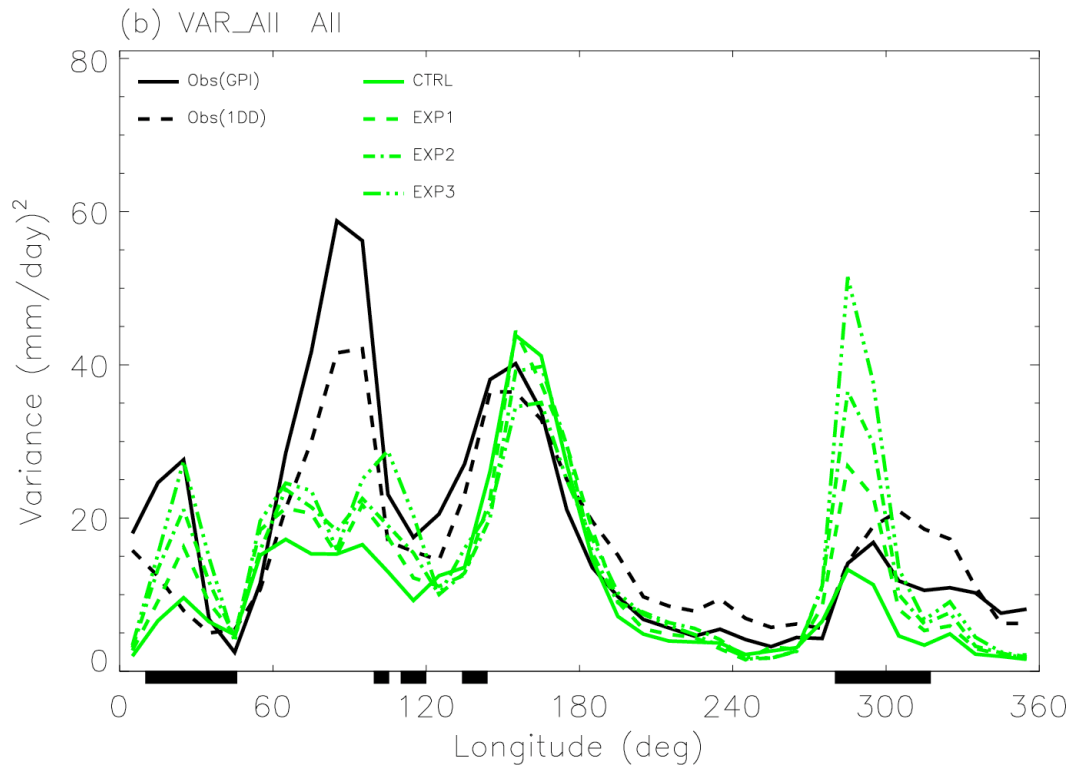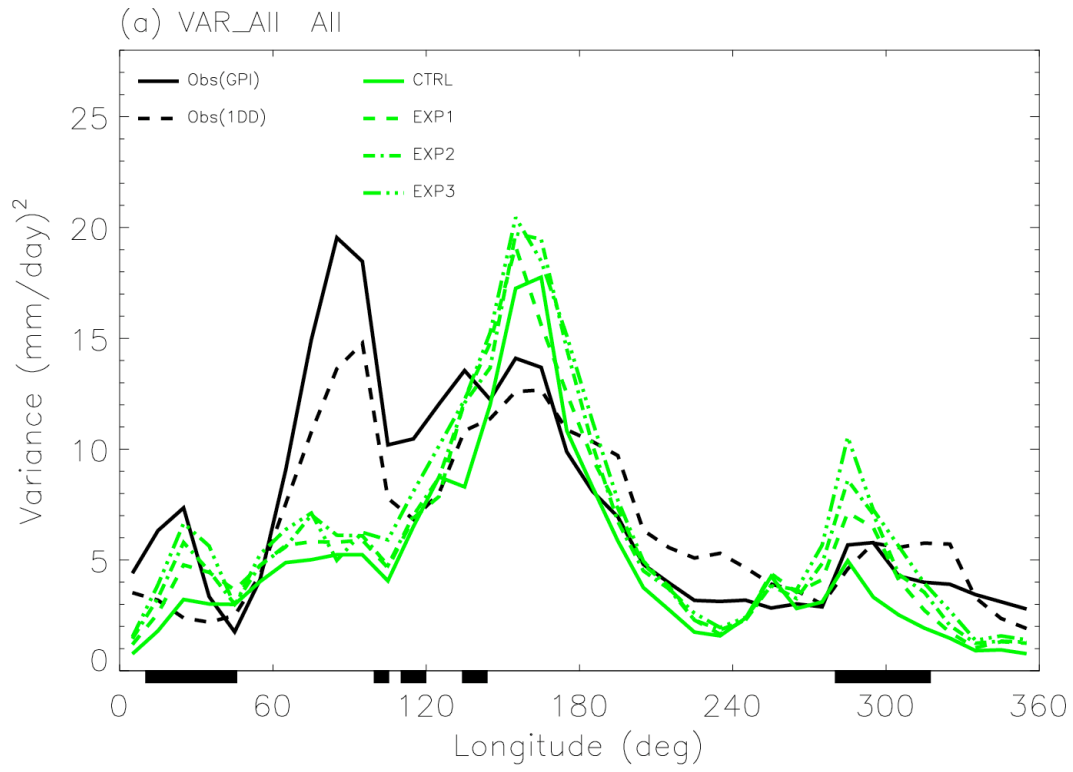
Figure 3. Variance of the 2-128 day precipitation anomaly along the equator averaged between (a) 15N-15S, and (b) 5N-5S.

Figure 4. Space-time spectrum of 15N-15S symmetric component of precipitation divided by the background spectrum. Superimposed are the dispersion curves of the odd meridional mode-numbered equatorial waves for the five equivalent depths of 12, 25, and 50m. Frequency spectral width is 1/128 cpd.

Figure 5. As in Figure 4 except for 15N-15S antisymmetric component of precipitation.

Figure 6. Variances of (a) MJO, (b) Kelvin, (c) ER, (d) MRG, (e) EIG, and (f) WIG modes along the equator averaged between 15N and 15S.

Table 1. Description of sensitivity experiments

Experiment	Autoconversion timescale (seconds)
CTRL	9600
EXP1	3600
EXP2	1800
EXP3	900

Figure 1. Linear regression of daily -OLR vs precipitation along the equator averaged between 5N-5S for observation and model experiments. Same unit is used for both variables so that the regression coefficient is unitless.

Figure 2. Annual mean precipitation along the equatorial belt averaged between (a) 15N and 15S, and (b) 5N and 5S for two observational datasets and each model experiment. The data are smoothed zonally to keep only wavenumber 0-6. The locations of continents within the equatorial belt are indicated by black bars under the abscissa.

29

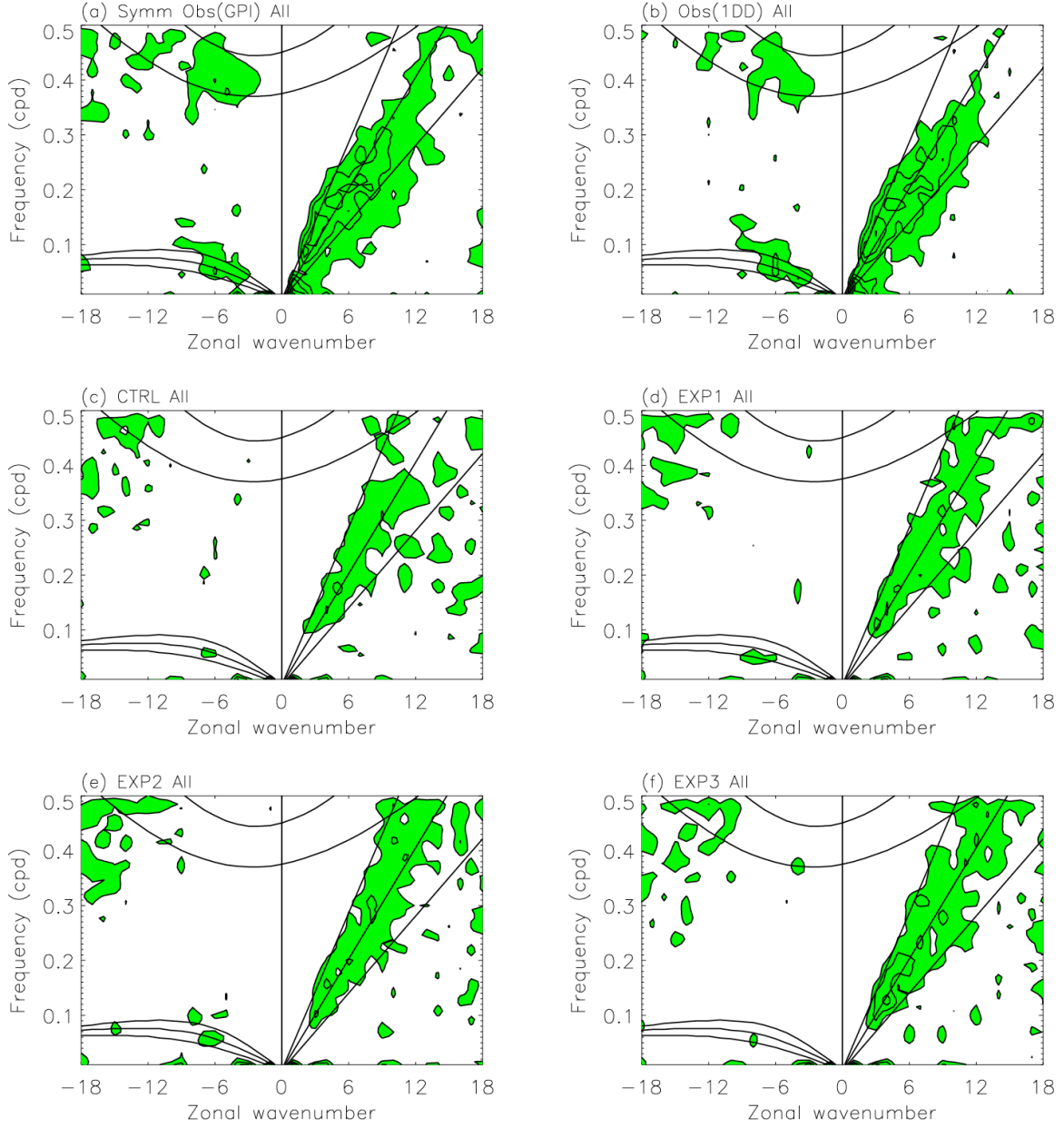Figure 3. Variance of the 2-128 day precipitation anomaly along the equator averaged between (a) 15N-15S, and (b) 5N-5S.

Figure 4. Space-time spectrum of 15N-15S symmetric component of precipitation divided by the background spectrum. Superimposed are the dispersion curves of the odd meridional mode-numbered equatorial waves for the five equivalent depths of 12, 25, and 50m. Frequency spectral width is 1/128 cpd.
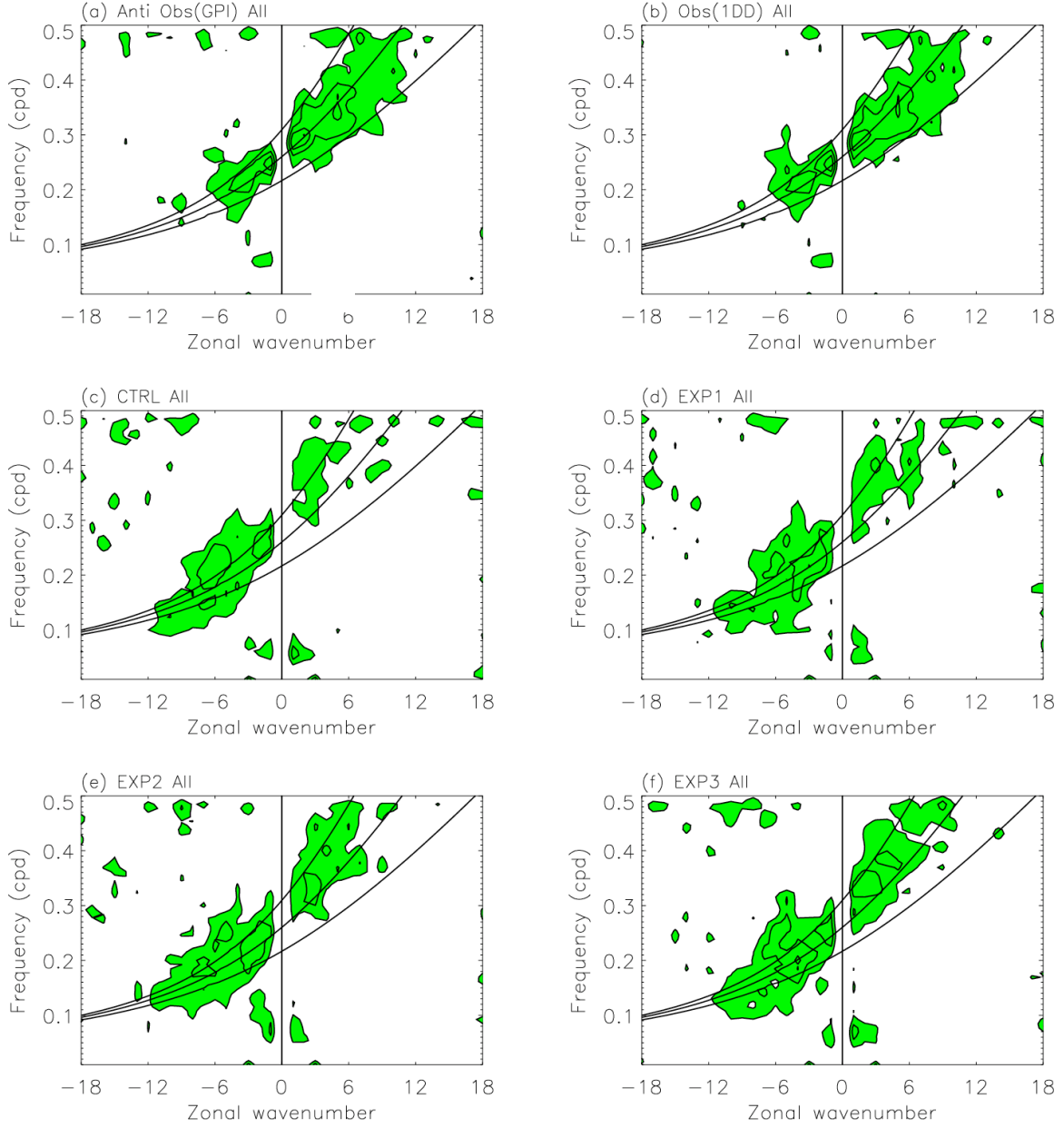
Figure 5. As in Figure 4 except for 15N-15S antisymmetric component of precipitation.
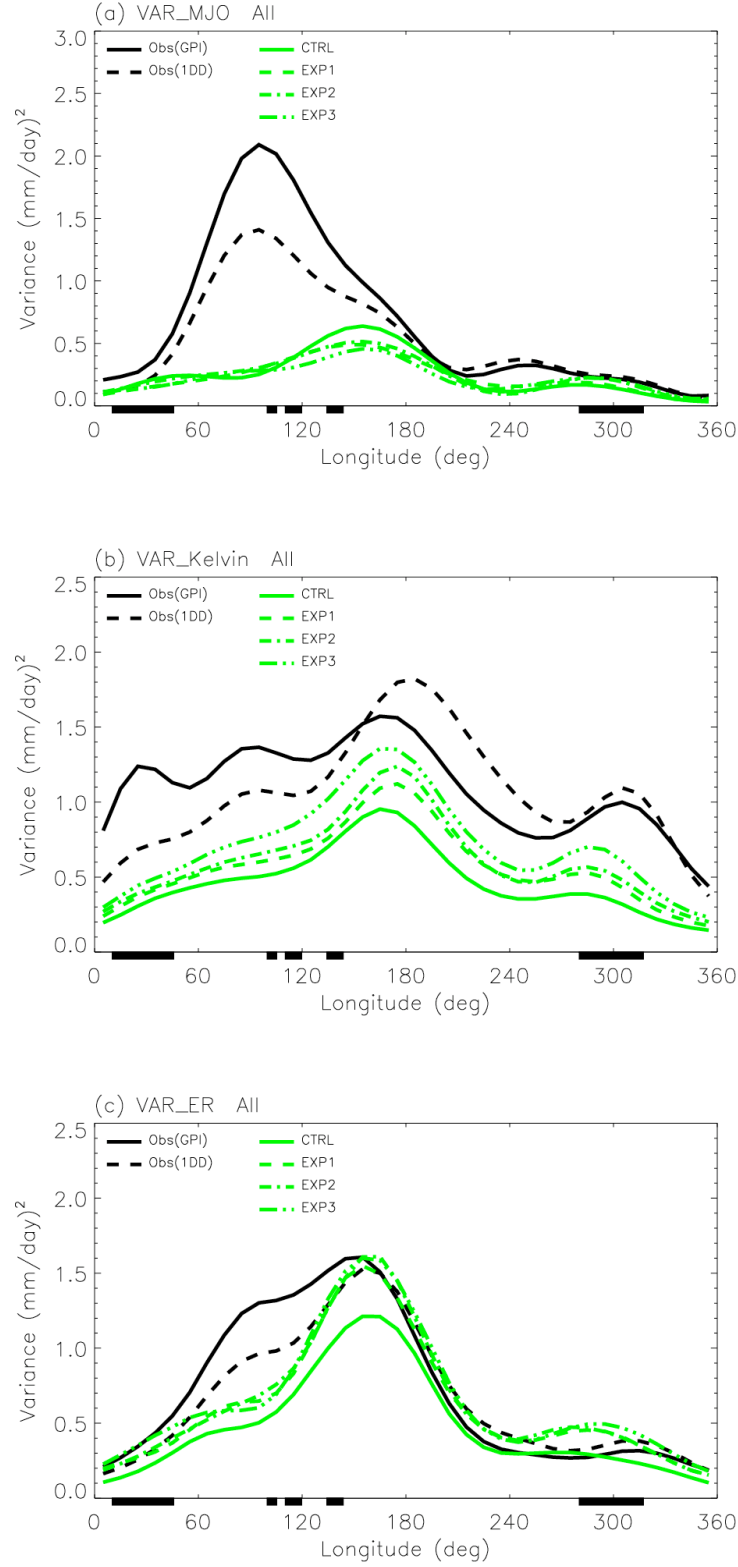
Figure 6. Variances of (a) MJO, (b) Kelvin, (c) ER, (d) MRG, (e) EIG, and (f) WIG modes along the equator averaged between 15N and 15S.
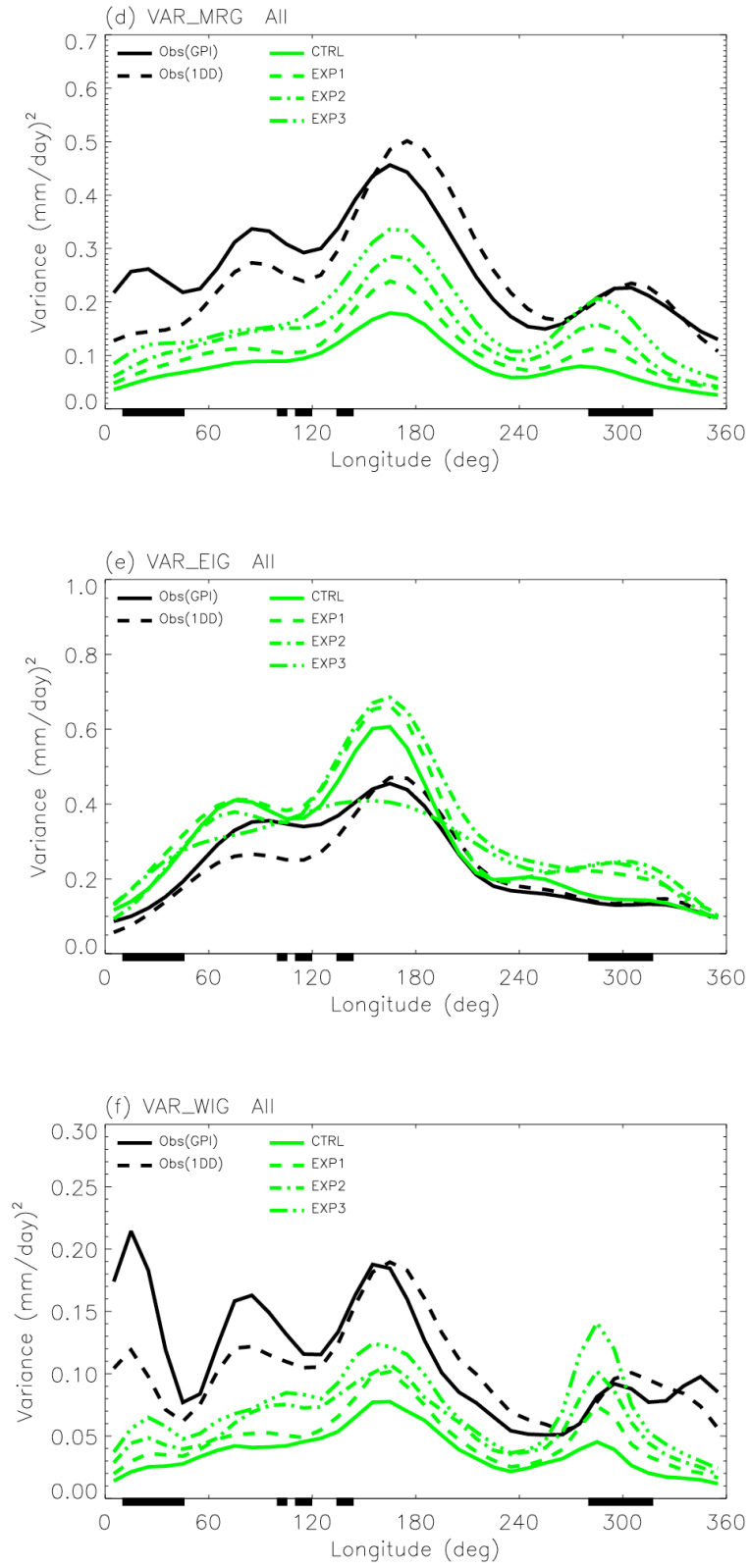
Figure 6. Continued.